JOURNAL OF GEOPHYSICAL RESEARCH, VOL. 108, NO. D22, 8856, doi:10.1029/2002JDO03124, 2003

Spatial patterns of soil moisture connected to monthly-seasonal precipitation variability in a monsoon region

Yongqiang Liu[1]

School of Earth and Atmospheric Sciences, Georgia Institute of Technology, Atlanta, Georgia, USA

Received 31 October 2002; revised 1 July 2003; accepted 30 July 2003; published 8 November 2003.

[1] The relations between monthly-seasonal soil moisture and precipitation variability are investigated by identifying the coupled patterns of the two hydrological fields using singular value decomposition (SVD). SVD is a technique of principal component analysis similar to empirical orthogonal functions (EOF). However, it is applied to two variables simultaneously and is capable of extracting spatial patterns of one variable which are closely connected to variability of the other. Simulation is performed with a regional climate model to reproduce soil moisture and precipitation in east Asia. It is found that, of a number of leading soil moisture SVD patterns, those representing meridional anomalies have closer relationships to subsequent precipitation variability. The corresponding atmospheric variability is characterized by opposite anomalies between the middle and low troposphere and by comparable anomalies between the middle and low latitudes. These patterns occur more frequently during spring and summer. The time lag correlations of the SVD expansion series with soil moisture leading precipitation are much greater than those of the original data series and EOF expansion series, suggesting that predictability of monthly-seasonal precipitation variability could be improved by using soil moisture in the form of its coupled SVD patterns with precipitation. *INDEX TERMS:* 1866 Hydrology: Soil moisture; 1854 Hydrology: Precipitation (3354); 3322 Meteorology and Atmospheric Dynamics: Land/atmosphere interactions; 3337 Meteorology and Atmospheric Dynamics: Numerical modeling and data assimilation; *KEYWORDS:* soil moisture, precipitation, coupled patterns

Citation: Liu, Y., Spatial patterns of soil moisture connected to monthly-seasonal precipitation variability in a monsoon region, *J. Geophys. Res.*, *108*(D22), 8856, doi:10.1029/2002JD003124, 2003.

1. Introduction

[2] Soil moisture controls water and energy exchanges by providing available water for evapotranspiration and by determining the partition of radiative energy absorbed on the ground surface into sensible and latent heat fluxes [*Avissar*, 1995]. Therefore anomalies in soil moisture can result in significant changes in atmospheric hydrological and thermal processes by land-atmospheric interactions. A large number of studies have indicated the importance of soil moisture in weather and climate anomalies [e.g., *Mintz*, 1984; *Dickinson and Henderson-Sellers*, 1988; *Avissar and Verstraete*, 1990; *Koster and Suarez*, 1995; *Betts et al.*, 1996; *Avissar and Liu*, 1996].

[3] An important property of soil moisture is the capacity to retain anomalous signals over long periods. Anomalies in soil moisture can persist from months to seasons [e.g., *Delworth and Manabe*, 1988, 1989; *Vinnikov et al.*, 1996; *Liu and Avissar*, 1999a, 1999b]. As a result, soil moisture can contribute to long-term atmospheric variability over land by passing its relatively slow anomalous signals to the atmosphere. Some relationships have been obtained between soil moisture with subsequent monthly-seasonal variability in air temperature and other atmospheric variables at the surface [e.g., *Karl*, 1986; *Huang et al.*, 1996; *Wang and Kumar*, 1998].

[4] Regional climate models (RCMs), first developed at the National Center for Atmospheric Research (NCAR) in the late 1980s [e.g., *Giorgi and Bates*, 1989; *Dickinson et al.*, 1989], have emerged as an important tool for investigating the relationships of soil moisture to regional weather and climate anomalies, including severe floods and droughts. *Giorgi et al.* [1996] investigated the role of soil moisture-rainfall feedback in the 1988 drought and the 1993 flood in the midwest United States. *Hong and Pan* [2000] and *Pal and Eltahir* [2001] further examined the two events and proposed different mechanisms. *Bosilovich and Sun* [1999] examined the 1993 flood in the midwest United States and pointed out that the changed moisture convergence within the flood region, connected to the change in the low-level jet induced by soil moisture anomalies, was a major mechanism for the rainfall increase. *Schar et al.* [1999] found a similar mechanism in simulations over Europe. *Liu et al.* [1996] modeled the 1991 flood event in central China with the NCAR regional climate model (RegCM). *Seth and Giorgi* [1998] further examined the effects of domain choice on the simulations reported in the work of *Giorgi et al.* [1996] and

[1]Now at Forestry Sciences Laboratory, USDA Forest Service, Athens, Georgia, USA.

Copyright 2003 by the American Geophysical Union.
0148-0227/03/2002JD003124$09.00

showed that a smaller domain captured observed precipitation better in the upper Mississippi basin but the sensitivity of precipitation to initial soil moisture appears to be more realistic in a larger domain. *Giorgi and Bi* [2000] investigated internal variability and showed that perturbations grow in the first 5–15 days but do not continue to diverge.

[5] Understanding of the importance of soil moisture to precipitation variability has been an objective of a number of research programs and activities. A great effort has been made as part of the Global Energy and Water Cycle Experiment (GEWEX) to conduct field measurements and to develop models for studying soil moisture and its interactions with the atmospheric processes. An additional goal of the GEWEX America Prediction Project (GEWEX Americas Prediction Project (GAPP) Science Plan and Implementation Strategy, 159 pp., 2000) was to develop and demonstrate a capability in making reliable monthly and seasonal predictions of precipitation and land-surface hydrologic processes using soil memory. The National Center for Environmental Prediction (NCEP) explored the potential to predict summer precipitation over the United States using the ensemble canonical correlation technique with soil moisture as one of the predictors [*Mo*, 2002].

[6] Because of the extreme complexity in precipitation and soil moisture variability, and in land-atmosphere interactions, relations of soil moisture to subsequent precipitation variability are significant only under certain circumstances. Various approaches have been applied to identifying such circumstances. It was found that soil moisture persistence is more significant in high latitudes, during winter seasons, or in dry climate regions [*Delworth and Manabe*, 1988, 1989; *Liu and Avissar*, 1999a]. The foreknowledge of land surface moisture state contributes significantly to predictability in transition zones between dry and humid climates [*Koster et al.*, 2000]. A number of feedback mechanisms could retain and amplify anomaly signals in soil moisture and the atmosphere [e.g., *Rodriguez-Iturbe et al.*, 1991; *Entekhabi et al.*, 1992; *Brubaker and Entekhabi*, 1996; *Findell and Eltahir*, 1997; *Eltahir*, 1998; *Liu and Avissar*, 1999b]. Recent observational analyses of soil moisture measurements determined a spatial scale, at which interactions between soil moisture and the large-scale atmospheric processes become important [*Entin et al.*, 2000; *Liu et al.*, 2001].

[7] This study examines the circumstances by identifying the spatial patterns of soil moisture which are closely connected to monthly-seasonal precipitation variability. A regional climate model is used to simulate the land-atmospheric system of east Asia, the location of one of the GEWEX study areas (GEWEX Asian Monsoon Experiment or GAME). The simulated soil moisture and precipitation are analyzed using singular value decomposition (SVD). The simulation and SVD analysis are first briefly described in the next section. The leading SVD patterns of soil moisture, temporal relations, and the significance to prediction of precipitation variability are presented in the sections 3–5. Concluding remarks are given in the final section.

2. Methodology

2.1. Simulation

[8] The second version of NCAR RegCM [*Giorgi et al.*, 1993a, 1993b] with modified explicit rainfall calculation

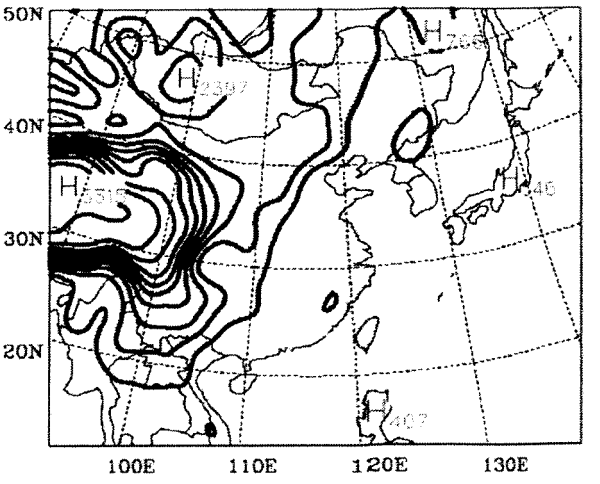

Figure 1. Regional model domain and topography. The contour interval is 500 m.

[*Giorgi and Shields*, 1999] was used to simulate variations in the east Asian land-atmospheric system. RegCM characterizes regional features of climate and land-surface processes at geographic regions of interest by incorporating improved schemes of a number of critically important climate processes, including Biosphere-Atmosphere Transfer Scheme (BATS) land-surface physics [*Dickinson et al.*, 1993] and the NCAR radiative transfer model [*Kiehl et al.*, 1996], into the standard NCAR/Pennsylvania State University Mesoscale Model Version 4 (MM4) [*Anthes et al.*, 1987]. The Kuo-type subgrid convective scheme [*Anthes*, 1977] was utilized. The model simulates snow when the temperature is below 0°C. The rate of change in snow cover is determined by the balance among the snow precipitation rate, snowmelting rate and the rate of sublimation. Snowmelting happens when the snow temperature (the same as the temperature of the upper layer of soil) is above 0°C. Snowmelting is estimated from the energy required to balance the net surface heating and lower the temperature to 0°C. RegCM was able to reproduce some important high-resolution spatial characteristics of climate for major geographic regions over the world, including east Asia [e.g., *Liu et al.*, 1996; *Lee and Suh*, 2000].

[9] Figure 1 shows the simulation domain and topography. The Tibetan Plateau stretches into the domain with a maximum height over 5 km. The domain is centered at 34°N and 116°E. It contains 90 by 79 grid points with a horizontal resolution of 60 km. There are 14 vertical layers with the top model atmosphere at 80 hPa. The initial and horizontal lateral boundary conditions of wind, temperature, water vapor, and surface pressure were interpolated from the analysis of the European Center for Medium-Range Weather Forecast (ECMWF), whose resolution is 1.875° of latitude and longitude (roughly 200 by 175 km at midlatitudes). Soil water content was initialized as described in the work of *Giorgi and Bates* [1989], i.e., the initial soil moisture content depends on the specified type of vegetation. Time-dependent sea-surface temperature (SST) was interpolated from a set of observed, monthly mean with a resolution of 1° [*Shea et al.*, 1992]. A data set of precipi-

tation from NCEP was used to validate rainfall simulation. All these data were obtained from archives of the NCAR Scientific Computing Division. Land type is specified based on the global 1-km resolution International Geosphere Biosphere Program (IGBP) land cover data set [*Zeng et al.*, 2000]. The integration period is from January 1987 to December 1997 with a time step of 3 min. The first year is considered as the spin-up period and, hence, excluded from the data series used in the SVD analysis. We will refer to the last 10 years as the simulation period.

[10] A global circulation model (GCM) could be an alternate tool to produce soil moisture and precipitation needed for the SVD analysis. A RCM has been used mainly in the consideration that, with the boundary conditions updated every 12 hours during the integration period using "observational data" (actually a combination of observation data and model outputs), a RCM is expected to produce relatively realistic regional circulation patterns. In addition, with a higher horizontal resolution of about 50 km, the effects of the ground forcing could be better captured by a RCM.

[11] *Giorgi and Mearns* [1999] discussed a number of factors affecting the performance of a RCM simulation, some of which are especially important to the simulation performed here. Most of the western boundary of the domain is over the Tibetan Plateau. This creates difficulties in generating reliable boundary conditions over the area. Some large errors are expected, mainly for summer monsoon periods. During winter monsoon periods (October through March), the Euro-Asian westerly, a major planetary-scale system, is located north to the Plateau. During the remainder of the year, however, the westerlies split into two branches, one remaining north of the Plateau (but much closer than during winter monsoon) and the other located south of the plateau. The southern branch of the western system generates synoptic and mesoscale weather systems. Low-level jets associated with these systems transport water vapor from the Indian Ocean, and bring rainfall to the southern and central China. As indicated in the next section, the model overpredicts the intensity of the surface low over the Tibetan Plateau and rainfall in central China, This may be related to the problem of the Tibetan Plateau being part of the western boundary. This problem can not be overcome simply by moving the bound of the domain westward. The Tibetan Plateau is too large.

[12] Domain size and internal variability created by disturbances in initial and boundary conditions are two other important issues. *Seth and Giorgi* [1998] indicated that RegCM produced more realistic response to internal forcing with a larger domain, but a better overall simulation with a small domain. *Giorgi and Bi* [2000] found that perturbations in initial and boundary conditions with RegCM grow in the first 5–15 days but do not continue to diverge. Finally, because of the need for large computing resources due to relatively short time step, RCMs, unlike most GCMs, usually are integrated over a short period up to a few years. This may adversely impact statistical assessments of simulation results.

[13] No attempts were made to evaluate sensitivity of the RegCM simulation in this study to these factors. It is implied from the study by *Giorgi and Bi* [2000] that the effects of internal variability related to initial and boundary perturbations on the simulation might be limited because of the long period of integration of the simulation.

2.2. SVD Analysis

[14] SVD is a technique to identify coupled spatial patterns with the maximum temporal covariance between two fields. It has been applied to analyzing relations between sea surface temperature (SST) and a meteorological field such as air temperature, precipitation, geopotential height, or atmospheric heat energy [*Wallace et al.*, 1992; *Ting and Wang*, 1997; *Wang and Ting*, 2000; *Trenberth et al.*, 2002]. A detailed description of SVD was presented in the work of *Bretherton et al.* [1992].

[15] Denote two fields as $\boldsymbol{u}(t) = [u(x_k, t)]$ and $\boldsymbol{v}(t) = [v(y_l, t)]$, where x_k and y_l are space locations; $k = 1, 2, \ldots, M_x$, $l = 1, 2, \ldots, M_y$, and M_x and M_y are the number of space locations for $\boldsymbol{u}$ and $\boldsymbol{v}$, respectively; And t is time from 1 to N. SVD analysis separates each of the two fields into spatial patterns and temporal series,

$$\boldsymbol{u}(t) = \sum_{k=1}^{M} a_k(t)\boldsymbol{p}_k \tag{1}$$

$$\boldsymbol{v}(t) = \sum_{k=1}^{M} b_k(t)\boldsymbol{q}_k, \tag{2}$$

where $\boldsymbol{p}_k$ and $\boldsymbol{q}_k$ are spatial patterns (principal components); $a_k(t)$ and $b_k(t)$ are temporal series (expansion coefficients); M is the smaller of M_x and M_y. An SVD mode is composed of a spatial pattern and its corresponding temporal series.

[16] $\boldsymbol{p}_k$ and $\boldsymbol{q}_k$ are obtained as the eigenvectors (singular vectors) of $C_{uv}C_{uv}^T$ and $C_{uv}^TC_{uv}$, respectively, where C_{uv} is the cross covariance of $\boldsymbol{u}(t)$ and $\boldsymbol{v}(t)$. The correlation between a_k and b_k has the following feature: Assuming that the nonnegative eigenvalues (singular values) σ_k are in decreasing order (i.e., $\sigma_i \geq \sigma_j$ for $i < j$), then the correlation between a_i and b_i is greater than or equal to that of a_j and b_j. This means that the largest response occurs between the first pair of spatial patterns, the second largest response between the second pair, and so on. The first few pairs of modes are regarded as SVD leading modes.

[17] The contribution of the kth pattern to the total covariance of the two fields is measured by squared covariance function (SCF),

$$SCF_k = \sigma_k^2 / \sum_{l=1}^{M} \sigma_l^2. \tag{3}$$

[18] Canonical correlation analysis (CCA) is a similar and more popular technique to identify coupled patterns of two fields. Major features are common between SVD and CCA. SVD was used for this study basically due to the consideration of SVD's features in prediction application. According to *Barnston* [1994], SVD is favored when a predictor and a predictand participating in each pattern linkage are similar to those found in the individual data set EOF patterns. In this analysis, soil moisture is considered as a potential predictor for prediction of precipitation

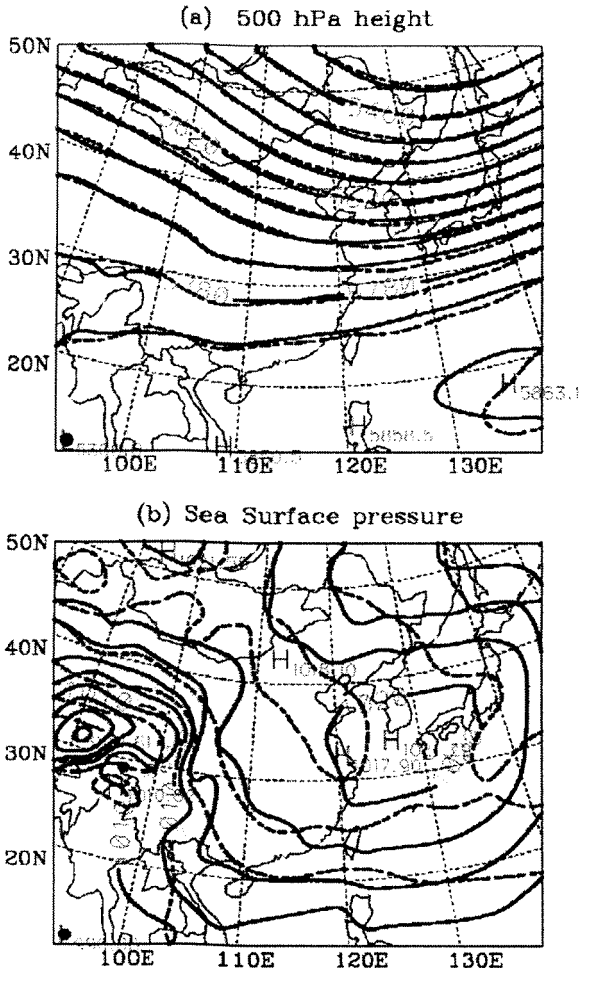

Figure 2. (a) 500 hPa geopotential height and (b) sea surface pressure. The solid and dashed lines represent RegCM simulation and ECMWF data analysis, respectively. The units are m (Figure 2a) and hPa (Figure 2b), and contour intervals are 40 m (Figure 2a) and 2.5 hPa (Figure 2b).

(predictand). As shown later, there is similarity between the SVD patterns of the two fields and their individual EOF patterns.

[19] The data series used in the SVD analysis are monthly means of soil moisture and precipitation simulated with RegCM. The values at every other grid point within the area of 80–135°E and 18–50°N were used. BATS has three layers—upper soil, root zone, and total soil. The upper and total soil layers have the fixed depth of 0.1 and 3 m, respectively. The depth of root zone varies from 1 to 2 m, depending on vegetation type of a grid. These three layers correspond to daily, intra-annual, and interannual processes, respectively. Soil moisture of root zone was used for the SVD analysis because monthly-seasonal variability is the concern of this study. Note that the properties of soil moisture seasonal variability, such as, timescales and persistence, vary with depth of soil [e.g., *Entin et al.*, 2000]. BATS has very limited capacity to address this issue because of its low vertical resolution. Simulation with a regional climate model coupled with a multilayer soil model [e.g., *Dai et al.*, 2003] should provide a solution to this problem.

3. Spatial Patterns

3.1. Simulated Fields

[20] Before the SVD results are described, a discussion of the atmospheric circulation and hydrology of east Asia for the simulation period is first provided. For the convenience of description, the portion of the analysis area within China is divided into south (south of 25°N), central (25–35°N), north (35–42°N), and northeast (42–52°N) China. The first three regions have humid, semihumid, and semiarid climate, respectively, and northeast China has semihumid climate. Mongolia, west to northeast China, belongs to semiarid and arid climate in its eastern and western portions, respectively.

[21] Figure 2 shows the simulated 500 hPa geopotential height and sea surface pressure averaged over the simulation period. There are two planetary-scale circulation systems. One is the east Asian trough in the middle latitudes. The trough line spreads from northeast southwestward down to the middle central China. The other is the northwestern Pacific subtropical high. Its center is located south of 20°N. There are also two systems on the ground: a high over most part of the domain and a low over the Tibetan Plateau.

[22] During a normal summer monsoon season from April to September, the Pacific high gradually moves northwestward [*Ding*, 1991]. Water vapor is transported from the Pacific Ocean to eastern China, Korea, and Japan by southeasterly flow in the southwestern sector of the high. Between the high and the midlatitude trough are the monsoon fronts, which are the major synoptic systems to produce precipitation. However, the circulation systems have large variability. Large variance in 500 hPa geopotential height during the simulation period occurs in the pretrough area over Japan, corresponding to the northwest Pacific storm track (not shown). Another area with large variance is in western central China, where the mesoscale or synoptic systems that originate over the Tibetan Plateau move eastward during summer seasons.

[23] The simulated 500 hPa geopotential height is very close to the ECMWF data analysis in spite of a little bit stronger Pacific high. There is a general similarity in the spatial patterns between the simulated and analyzed sea surface pressure. However, the magnitude of the low over the Tibetan Plateau is oversimulated, and the two separate highs over north China (centered at about 40°N, 115°E) and north Japan (the upper right corner of the domain) in the analysis data merge into a stronger single high centered over the ocean south to Korea in the simulation.

[24] The distributions of precipitation and soil moisture in China averaged over the simulation period (Figure 3) are basically in accordance with the climatological regions, as described above. A large amount of annual rainfall of about 2000 mm over south and central China is produced by the atmospheric disturbances associated with the east Asian trough and water vapor transport from the low latitudes. Rainfall decreases toward north China, which has the annual amount of only 250 mm. Northeast China, on the other hand, has more rainfall than north China. Similar to

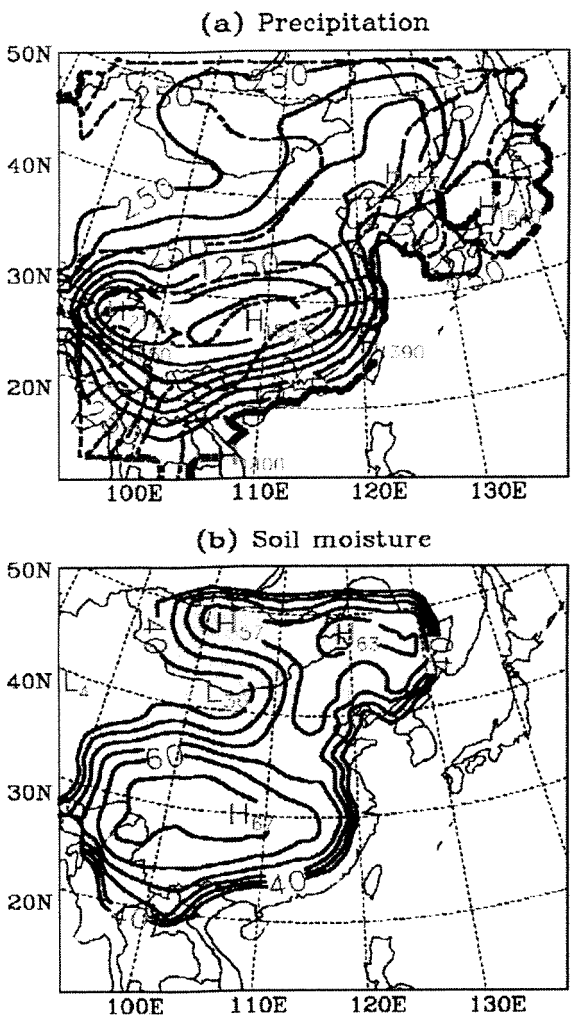

Figure 3. (a) Annual rainfall and (b) soil moisture of the root-zone layer relative to saturation. The solid and dashed lines represent RegCM simulation and observation, respectively. The units are mm (Figure 3a) and % (Figure 3b), and the contour intervals are 250 mm (Figure 3a) and 5% (Figure 3b).

precipitation, soil moisture first decreases from south to north China, and then increases toward northeast China. Some centers of over 60% occur in central and northeast China. The driest area is in the western north China, where soil moisture is about half of that in the moist areas.

[25] Owing to the direct relation to the east Asian monsoon, which has large interannual variability, the standard deviation of annual rainfall is as large as 700 mm, or one third of the average (not shown). The standard deviation of soil moisture, on the other hand, is relatively small, only about 10% of the average in south, central and northeast China. The smaller ratio of standard deviation of soil moisture than precipitation may suggest the important roles of evapotranspiration and runoff in soil moisture variability. Although soil moisture variations are directly controlled by rainfall, evapotranspiration and runoff play a role in resisting the tendency in soil moisture variations. For example, a wet (dry) soil will lead to large (small) evapotranspiration, which in turn reduces (increases) soil moisture. In addition, the water exchange between root-zone and deep soil also prevents soil moisture anomalies of root-zone layer from continuous growth. The smaller ratio may also suggest less sensitivity of BATS to the forcing from rainfall variability at the monthly-seasonal scales.

[26] The spatial patterns of the simulated and observed precipitation are similar to each other. However, there are two major deficiencies with the simulation: The model overestimates rainfall over most of the continental, and the maximum rainfall area shifts northwestward from the southeastern coastal region. The abnormally strong high in the simulated sea surface pressure and 500 hPa geopotential height should be one of the responsible factors.

[27] *Entin et al.* [2000] and *Liu et al.* [2001] analyzed spatial patterns of soil moisture in China. *Liu et al.* [2001] used the measurements of top 1-m layer for the period of 1981–1991. Although continuous distribution was not available because of the sparse measurement sites, their results showed large soil moisture over 240 mm in south China and northeast China, and small soil moisture below 40 mm in the western north China. It seems that the model is able to reproduce this pattern. As mentioned before, the root-zone depth varies with vegetation type. To roughly compare the magnitude with the measurements, the simulated soil moisture of root-zone layer (in mm) is converted into the equivalent values of a "1-m layer" by dividing the depth of the root-zone layer. The magnitude of soil moisture of the "1-m layer" is about 300 mm in south, central, and northeast China, and about 60 mm in the western north China. So the simulated magnitude is about 25% more than that of the measurements in the moist regions. The overestimation of soil moisture should be related to the overestimated rainfall by the model.

3.2. SVD Patterns

[28] Soil moisture ($\boldsymbol{u}$) and precipitation ($\boldsymbol{v}$) of each month were first normalized by subtracting their respective multiyear average divided by mean squared root of that month, which was expected to have a major portion of seasonal cycle removed. SVD then was applied to the series. Figure 4 shows the first four SVD leading patterns of soil moisture ($\boldsymbol{p}_k$), which are multiplied by their corresponding singular value (σ_k). The 1st soil moisture mode consists of a pair of positive and negative anomalies separated between 32–35°N. The anomalous regions are basically zonally oriented. Each region has a size about 30 degrees × 15 degrees, equivalent to the size of about 3000 by 1500 km. The 2nd mode represents a pattern of more or less meridionally oriented anomalies. There are two areas of negative anomalies, one spreading from Mongolia and northeast China down southwestward to central China, and the other in the western south China. In between are positive anomalies with two centers located in the coastal south China and the western north China. The size of the anomalies in Mongolia-northeast China area is comparable to that of the 1st mode, while that in other regions is reduced by about half. The 3rd mode is similar to the 2nd mode in terms of its meridional orientation. However, the negative anomalies in the north do not spread over Mongolia. The last mode

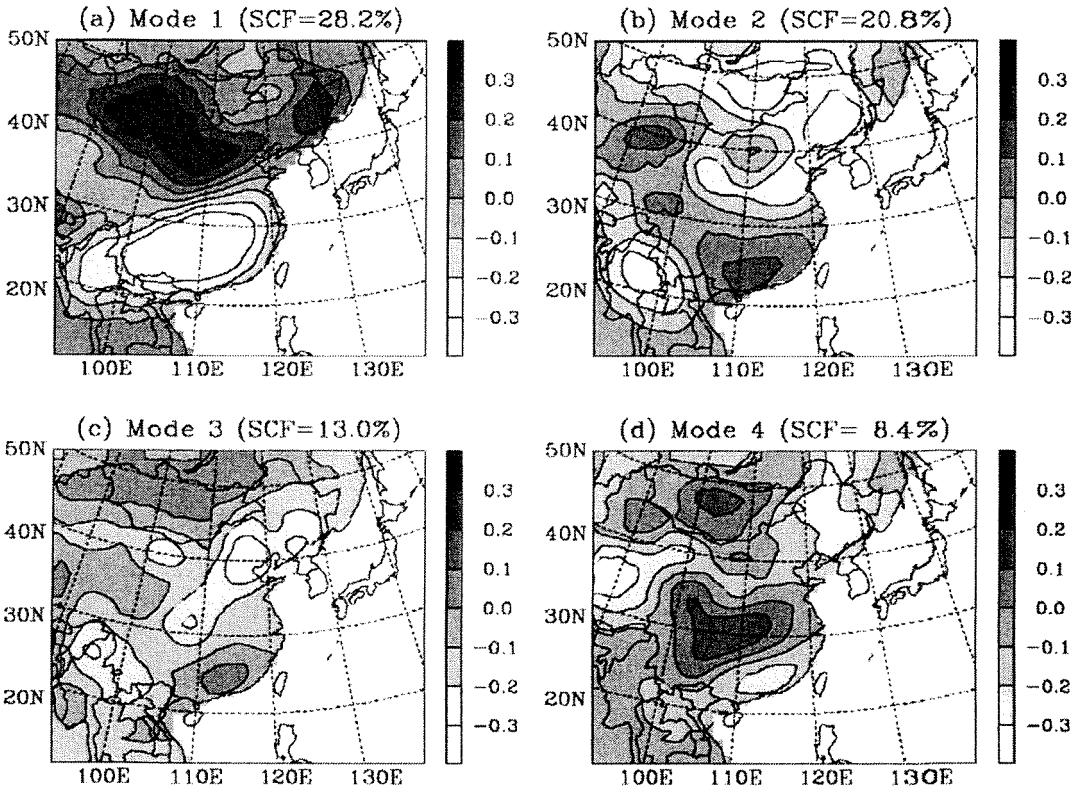

Figure 4. The four SVD leading patterns of soil moisture weighted by their corresponding singular values. SCF stands for squared covariance function. See color version of this figure in the HTML.

contains positive anomalies in most areas, with weak negative anomalies occurring in the southeastern coastal area, northeast China, and the western boundary of the domain.

[29] SCFs of the four modes are about 28, 21, 13, and 8% (also see Table 1), and the accumulated SCF is about 70%. Physically, the values shown in Figure 4 represent correlation between soil moisture field and kth SVD expansion series of precipitation. The critical correlation coefficients, which are the minimum values for correlations to be statistically significant at specific confidence levels, are about 0.3 and 0.23 at the confidence levels of 99.9% and 99%, respectively. The anomaly centers of all the leading modes except the 3rd one reach the 99% confidence level. The variance of each of the four SVD expansion coefficient series accounts for from 6 to 16% of total variance of soil moisture. The accumulated contribution is about 45%. The corresponding value for precipitation is smaller with an accumulated contribution of about 26%. There are close relationships between each of the corresponding patterns. The correlation coefficients between soil moisture and precipitation for each pair of expansion coefficient series are from 57 to 78%.

[30] The SVD spatial patterns of precipitation (not shown) are mostly similar to those of soil moisture. This implies that the closest relations between soil moisture and precipitation would occur when their anomalous patterns are similar to each other and that the feedback between soil moisture and precipitation would be mostly positive at monthly-seasonal scales. Major differences are the negative anomalies of the 3rd mode moved up to Mongolia, and the positive anomalies of the 4th mode extended over a larger area.

3.3. Corresponding Atmospheric Patterns

[31] Regression analysis is a useful tool for understanding the physical processes responsible for coupled SVD patterns [*Wang and Ting*, 2000]. It was used in this study to find the corresponding atmospheric patterns to the soil moisture SVD patterns. Linear regression relations were established at each location between each of the four SVD leading modes and the 500 hPa geopotential height or sea level pressure. Considering the seasonal dependence of the SVD modes, which will be described in the next section, the regression analysis was done only for two seasons of a year when the spatial correlation between soil moisture and an SVD leading pattern is significant. The chosen seasons are fall and winter (September through February) for the 1st mode, and spring and summer (March through August) for the other modes. Figure 5 shows the regression relations, expressed by correlation coefficients, between soil moisture SVD modes and the atmospheric anomalous fields.

[32] For the 500 hPa geopotential height, strong regression relations for the 1st and 4th SVD modes occur mainly in middle latitudes, where the atmosphere is controlled by the east Asian trough. This suggests that variability with the

Table 1. Statistics of the Four SVD Leading Modes of Soil Moisture (S) and Precipitation (P)[a]

Modes	SCF, %	σ_S, %	σ_P, %	$r_{S,P}$, %
1	28.2	13.4	9.1	65.8
2	20.8	10.0	6.4	77.7
3	13.0	15.8	4.7	57.4
4	8.4	5.8	6.3	65.3

[a] *SCF*, σ, and $r_{S,P}$ represent squared covariance function, variance ratio of an SVD expansion coefficient series to original data series, and correlation coefficient of SVD expansion coefficient series between *S* and *P*, respectively.

trough would be primarily responsible for the generation of the two soil moisture SVD modes. The regression relations for two other modes, on the other hand, are also considerable in south and central China, suggesting that variability in both the east Asian trough and the mesoscale and synoptic systems in the lower latitudes would be responsible for the generation of the two soil moisture modes.

[33] There are two types of vertical variations in the relations. The anomalies have the same signs between 500 hPa geopotential height and sea surface pressure for the 1st and 4th SVD modes. For the 1st mode, the signs of the regression coefficients are mostly negative at both elevations. The strongest connections occur over northeast China, a region with the middle-latitude trough in the atmospheric field (Figure 2) and extensive positive anomalies in the SVD pattern (Figure 4). Physically, a positive anomaly in the geopotential height (sea surface pressure) means a weaker trough, which leads to reduced precipitation and, therefore, negative anomalies in soil moisture. In this case, feedback of soil moisture to precipitation would be very weak (It will be seen in the next section that the relation

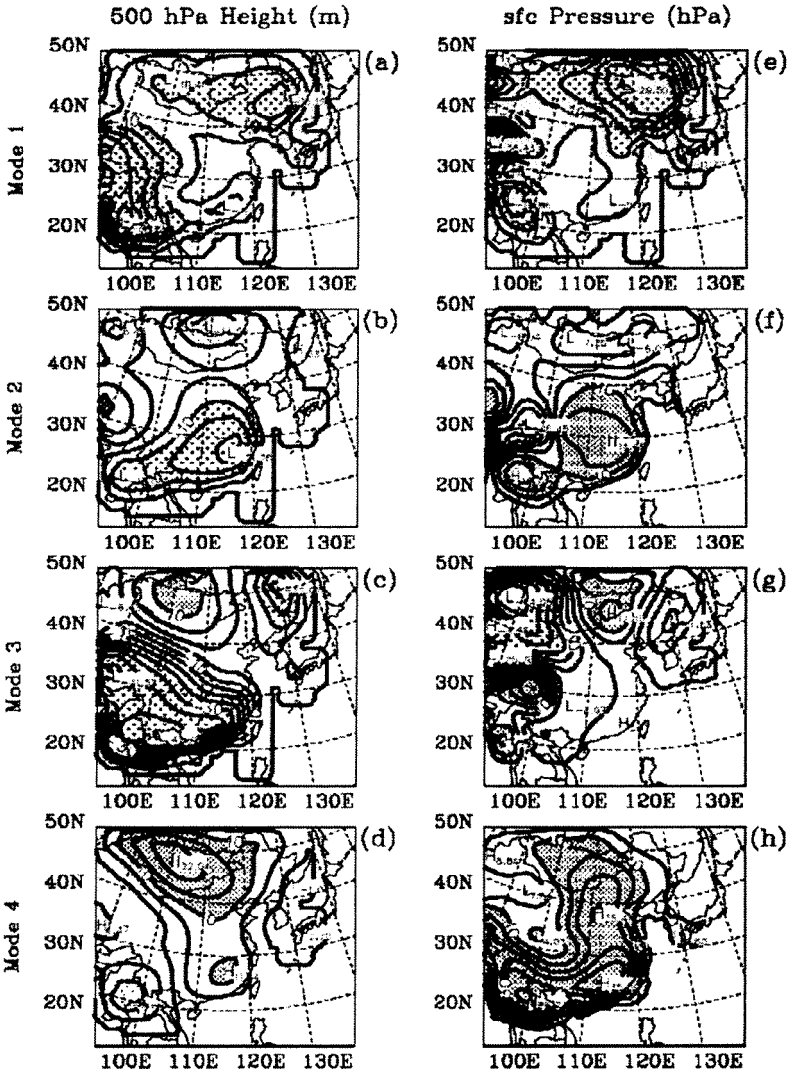

Figure 5. Regression relations of (left) the anomalous 500 hPa geopotential height and (right) sea surface pressure with the four SVD leading modes (from top to bottom). The dense and sparse dot shadings denote values above 10% and below −10%, respectively.

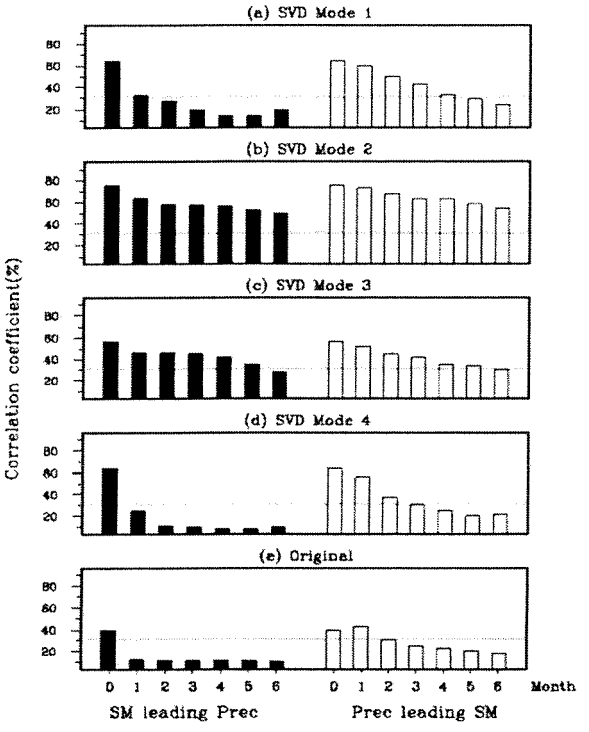

Figure 6. Time lag correlation coefficients between SVD expansion series for (left) soil moisture leading precipitation and (right) precipitation leading soil moisture. (a–d) The four SVD leading modes and (e) original data. The light line in each panel indicates the 99.9% confidence level.

of soil moisture to subsequent precipitation variability is relatively weak for this type of SVD modes). For the 4th mode, the signs are mostly positive at both elevations, though the areas with the strongest connections occur over the western Mongolia in 500 hPa geopotential height, but over the coastal China in sea surface pressure. For two other SVD modes, on the other hand, the regression shows opposite signs between the two elevations in some regions. For the 2nd mode, the regression coefficients are mostly negative in 500 hPa geopotential height and positive in sea surface pressure over the coastal areas; for the 3rd mode, the regression coefficients in the western north China are mostly positive in 500 hPa geopotential height and negative in sea surface pressure, and those in the other areas are mostly negative in 500 hPa geopotential height and positive in sea surface pressure.

[34] On the basis of their features of the corresponding atmospheric patterns, the four leading SVD soil moisture modes (both spatial patterns and time series) can be divided into two types. Type I consists of the 1st and 4th soil moisture SVD modes, whose corresponding atmospheric anomalous patterns are featured by strong connections in middle latitudes in the middle troposphere, and by the same signs of anomalies between the middle and low troposphere; type II consists of the 2nd and 3rd modes, whose corresponding atmospheric patterns are featured by comparable importance between the atmospheric systems in the middle and low latitudes and by opposite signs between the middle and low troposphere in some regions.

[35] *Entin et al.* [2000] and *Liu et al.* [2001] used spatial scale as a criteria to define soil moisture variability types which have different features in the interactions between soil moisture and the large-scale atmospheric processes. Here we category soil moisture variability into different types based on its spatial patterns and relations to the atmosphere. The analysis in the next section will show that the two types of soil moisture patterns have different features in the relations to subsequent precipitation variability.

4. Temporal Relations

[36] Figure 6 shows time lag correlation coefficients for the expansion coefficient series of the four leading SVD modes between soil moisture and precipitation. The correlation for kth series (k = 1, 4) with soil moisture leading precipitation was calculated by the formula $\sum_{t=1}^{N-m} a_k(t)\, b_k(t+m)$, with a and b normalized and m the time lag length in month. It measures how close an SVD soil moisture pattern is related to subsequent precipitation variability. The formula for the correlation with precipitation leading soil moisture is obtained by exchanging a and b.

[37] The correlations for the expansion coefficient series of type II SVD modes are larger than those of type I SVD modes. For type II, the correlation coefficients with soil moisture leading precipitation are significant for the lag time up to six months at the 99.9% confidence level (the critical correlation value is 30%). In contrast, those for type I are only barely significant for the lag time of one month at the confidence level. This result suggests that soil moisture could affect the subsequent precipitation at monthly-seasonal scales mainly for type II SVD soil moisture modes.

[38] There are also differences in the connections of precipitation to its subsequent variability, a measure of persistence of precipitation anomalies, between the two types of SVD modes. The persistence means that, if there are precipitation anomalies in a certain month, it is likely that the same anomalies would repeat in the following months. Persistence can be another factor for prediction of precipitation variability in addition to the relations between soil moisture and precipitation.

[39] Figure 7 displays the features of the persistence. It is measured by autocorrelation and calculated by the formula $\sum_{t=1}^{N-m} c_k(t)\, c_k(t+m)$, with c being either normalized a or b. Note that both this correlation and the time lag correlation described in Figure 6 measure relationship at two different times, but the former is between two variables, while the later is with one variable. Figure 7 does not display the coefficients of zero month lag, which always are 100%. Soil moisture shows strong persistence because of its long memory, consistent with the previous analyses [e.g., *Delworth and Manabe*, 1988, 1989; *Vinnikov et al.*, 1996; *Liu and Avissar*, 1999a, 1999b]. The persistence of precipitation is stronger for type II than type I SVD modes. The correlation coefficients are significant for time lags up to five (three) months for the series of the 2nd (3rd) SVD mode at the 99.9% confidence level. In contrast, they are not significant for the series of the 1st and 4th SVD modes except that of the 1st SVD mode with one-month lag.

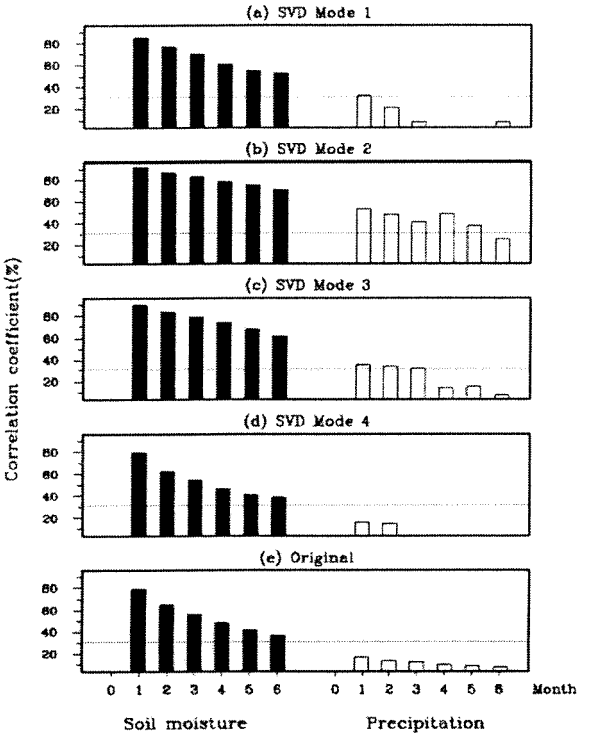

Figure 7. Same as Figure 6 except for autocorrelation coefficients.

[40] The above results indicate that, among the four leading SVD modes of soil moisture, only those of type II have close relationships to subsequent variability of precipitation. Some explanations can be obtained based on the features of their corresponding atmospheric patterns, that is, opposite signs of anomalies between the middle troposphere and the surface, and significant anomalies at both middle and low latitudes. Opposite anomalies between the middle and low troposphere is mostly generated by abnormal heating or cooling limited in the low troposphere, whose horizontal scale is small and life time is short. Thus the feature usually indicates weak control by an atmospheric system. As a result, soil moisture plays a relatively important role in variability of precipitation. In contrast, the same signs of atmospheric anomalies between the two heights for type I SVD patterns usually indicate strong control by an atmospheric system throughout entire troposphere. In this case soil moisture's role is less significant. The second feature may reflect a low westerly index, i.e., anomalously strong planetary-wave activities. This favors the development of synoptic systems which have small scales and move fast. Their effects on long-term atmospheric processes are very limited. As a result, the role of soil moisture becomes relatively important.

[41] Physical mechanisms responsible for the relationships of soil moisture with subsequent precipitation variability at monthly and seasonal scales were investigated by analyzing a numerical experiment with RegCM (Y. Q. Liu, personal communication, 2002). In the experiment initial soil moisture in China is specified with its wilting-point value and RegCM is run from May through August for each of the five years (1988–1992). The results suggest two mechanisms for the effects of the dry spring soil on summer precipitation. One is reduced water vapor transport from the surface to the cloud layer, which leads to reduction in large-scale rainfall. The other is intensified thermal instability due to more sensible heat flux from the surface, which leads to increase in convective rainfall. The overall rainfall is reduced. The first mechanism was found in the simulation with dry soil conditions in the central United States [*Giorgi et al.*, 1996]. Other mechanisms have been proposed. For example, *Eltahir* [1998] proposed positive feedback mechanisms linking soil moisture, PBL moist static energy, and rainfall. *Bosilovich and Sun* [1999] and *Schar et al.* [1999] found the relations of soil moisture anomalies to the low-level jet and horizontal water vapor convergence within the flood region.

[42] Note that, in comparison with precipitation, monthly-seasonal variability of soil moisture should have much higher predictability because of much stronger persistence of soil moisture (Figure 7) and larger correlations with precipitation leading soil moisture (Figure 6). In addition, the differences in the relationships of precipitation with subsequent soil moisture variability and in soil moisture persistence between the two types of spatial patterns are not obvious.

4.1. Seasonal Dependence

[43] Both soil moisture memory and the intensity of land-atmosphere interactions vary with season. The persistence of soil moisture is stronger during winter than summer seasons [*Delworth and Manabe*, 1988], while the effects of soil moisture on precipitation is more significant during warm than cool seasons because of larger rate of land-surface water and energy exchanges. This suggests that the SVD patterns could have different importance for variability of soil moisture and precipitation during various seasons of a year. To analyze the seasonal dependence, spatial correlation coefficients between each of soil moisture and precipitation and its four leading SVD patterns are calculated in the following steps: For each of the 12 months in a certain year, compute spatial correlation coefficients between soil moisture or precipitation field and each of its SVD patterns; Repeat the procedure over the 10 years of the simulated period; Then obtain the averages over the 10 years for each month. The results are shown in Figure 8. The critical correlation value for 99% confidence level is about 10%.

[44] The spatial correlation coefficients between soil moisture and the SVD patterns of type II modes are larger in spring and summer seasons, indicating more chance for this type of patterns to appear during the two seasons. This suggests that the intensity of land-atmosphere interactions should be a more important factor than persistence for the development of the SVD soil moisture patterns. On the other hand, the spatial correlation coefficients between soil moisture and its 1st SVD pattern are larger in winter and fall seasons. There is no clear seasonal dependence for the 4th mode.

[45] The spatial correlation coefficients between precipitation and its SVD patterns have generally similar features to those of soil moisture. One exception is that the coefficient for the 2nd mode has no significant seasonal depen-

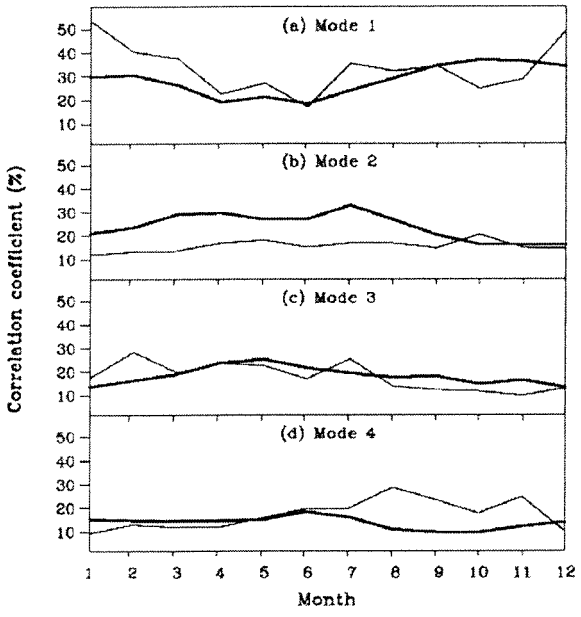

Figure 8. Seasonal variations of spatial correlation coefficients between a field and its four SVD leading modes (from top to bottom). The heavy and light lines represent soil moisture and precipitation, respectively.

dence. Another exception is the large correlations coefficients in summer and fall for the 4th mode.

4.2. Time Evolution

[46] Figure 9 shows the evolution of the SVD expansion coefficient series over the simulation period. The evolution is similar between soil moisture and precipitation. Among various scales with the expansion coefficient of the 1st mode is one-cycle variation. The negative and positive values occur during the first and second halves of the simulation period, respectively. This means that the pattern of dry anomalies in the southern portion of China and wet anomalies in the northern portion is dominant during the first half, while an opposite pattern is dominant in the second half (refer to Figure 4). The expansion coefficient for the 2nd soil moisture mode also has one-cycle variation but with different phase. Negative peak occurs in the middle, while positive peak occurs in the beginning and end of the simulation period. The variation may be of significance for prediction of decade-scale variability. It is possible that the one-cycle variation is part of a longer period of variation beyond the simulation period. Causes for the one-cycle variation need to be investigated for any possible implications.

[47] The variability of the SVD expansion coefficient series for the 3rd and 4th modes is more frequent, about three cycles over the simulation period. The peaks occur during the years of 1989, 1992, and 1997 for the 3rd mode, and 1988, 1993, and 1996 for the 4th mode. The frequency is comparable to that of the El Nino/La Nina events, which have periods of 2–5 years. The El Nino events during the simulation periods occurred during the years of 1991–1992, 1993, 1994, and 1997–1998, and the La Nina events occurred during 1988–1989 and 1995–1996. It seems there are no clear matches in the timing between the peaks/valleys of the SVD expansion coefficient series and the El Nino/La Nina events.

5. Predictive Significance of SVD Patterns

[48] We have analyzed two features of the SVD modes, that is, time lag correlation with soil moisture leading precipitation, and autocorrelation of precipitation. Here we compare with the corresponding features of original data series and EOF patterns to further illustrate the significance of the SVD patterns for prediction of monthly-seasonal precipitation variability.

5.1. Original Data Series

[49] The last panels of Figures 6 and 7 shows the time lag absolute correlation coefficients between soil moisture and precipitation, and the autocorrelation coefficients of soil moisture or precipitation of original data series, respectively. The method to obtain these coefficients are the same as those for the panels a–d of the corresponding figure except that the spatial average is made to the absolute values of the coefficients over all locations. Note the difference between the time lag correlation and autocorrelation as mentioned above.

[50] Although the simultaneous correlation coefficient (zero lag month) of 40% is comparable to those of the SVD leading modes, the correlation coefficients of the original data series with soil moisture leading precipitation by one month or longer are only about 15%. Meanwhile, the autocorrelation coefficients of the original precipitation series are much smaller than those of precipitation SVD

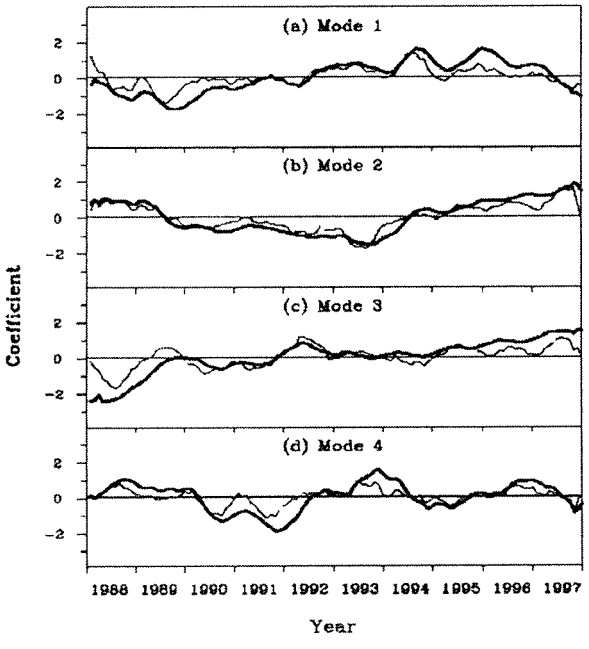

Figure 9. Temporal variations of the expansion coefficients of the four SVD leading modes (from top to bottom). The heavy and light lines represent soil moisture and precipitation, respectively.

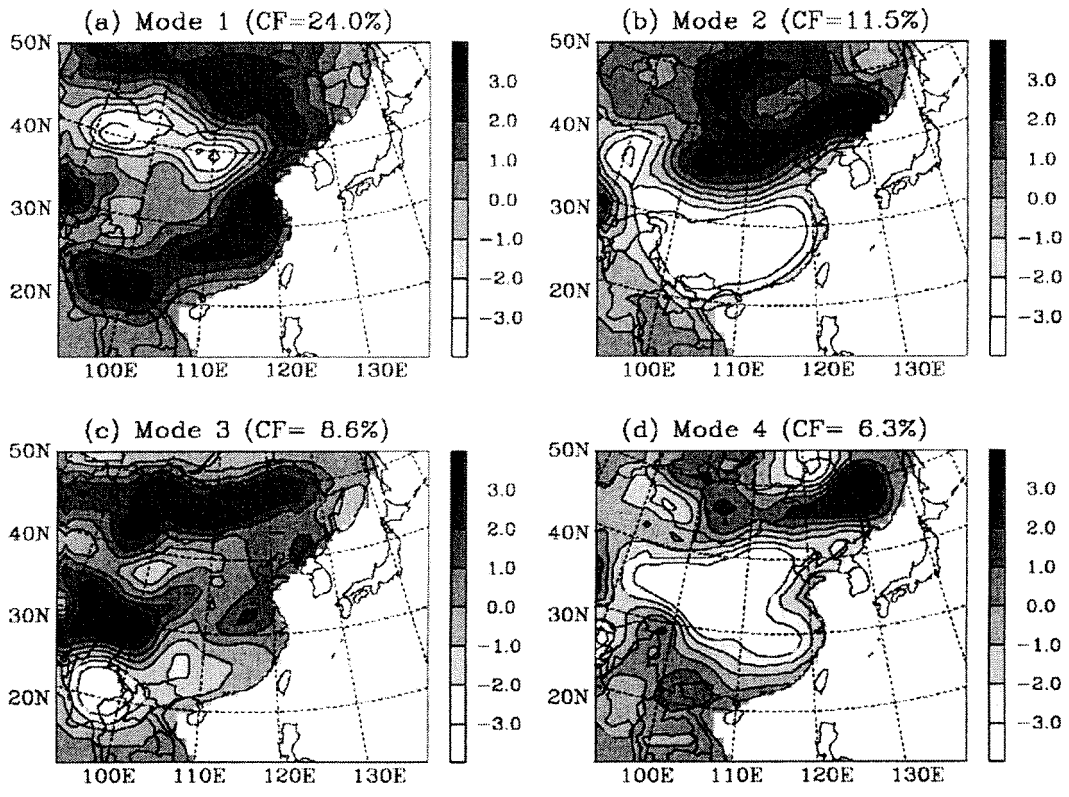

Figure 10. The four EOF leading patterns of soil moisture. CF stands for covariance function. See color version of this figure in the HTML.

expansion series. The one-month lag correlation coefficients, for example, are below 20% for the original data series, in comparison with about 30–50% for the 1st–3rd SVD modes.

[51] This result suggests that, if using soil moisture and/or precipitation as a predictor to forecast monthly-seasonal precipitation variability, a better predictability could be achieved by using the SVD patterns than original data at individual locations. Statistical prediction models could be developed on basis of the spatial patterns identified by the SVD analysis. A number of techniques are available for developing such models. One of them is to develop a statistical model using SVD spatial patterns of soil moisture as a predictor, similar to the method using CCA patterns [*Barnett and Preisendorfer*, 1987; *Barnston*, 1994]. An attempt was made in a recent study [*Liu*, 2003] to build such a model and to provide predictive evidence for the importance of the SVD soil moisture patterns in improving predictability of monthly-seasonal precipitation. The model is derived from a regression equation connecting the SVD patterns of soil moisture and precipitation. Skill of the model in predicting monthly and seasonal rainfall in the monsoon region of east Asia is evaluated by using a cross-validation method. The preliminary results do show some improvement in the predictability. The results, on the other hand, also indicate generally a low level of prediction skills.

[52] Another technique is ensemble forecast [*Mo*, 2002]. Soil moisture is used as one of predictors, together with sea surface temperature and other elements. SVD is performed for each predictor separately. An ensemble can be formed using the predicted monthly-seasonal precipitation from different predictors. This technique may have some advantages over a model with soil moisture used as only predictor and is expected to display better prediction skills.

[53] Note that, there is not much difference in the time lag correlation between precipitation and subsequent soil moisture variability and in the autocorrelation of soil moisture between the original data series and the SVD expansion series. This suggests less importance of the SVD patterns for prediction of monthly-seasonal soil moisture variability.

5.2. EOF Patterns

[54] EOF is a technique similar to SVD in terms of its role in identifying major spatial patterns. It has been extensively used in meteorological and hydrological analyses. *Wang and Kumar* [1998], for example, used EOF to analyze soil moisture patterns and the effects on variability of the surface climate in the United States. A difference from SVD is that it is only applied to one field.

[55] Figure 10 shows four leading EOF patterns of soil moisture. The 1st EOF pattern displays negative anomalies in the western China surrounded by positive ones in south, east, and north. The 2nd EOF pattern consists of a positive area in the north and a negative one in the south. The 3rd EOF pattern roughly has two pairs of positive and negative anomalies. And the last one is featured by dominant negative anomalies. The four EOF patterns contribute about 50% to total variance (Table 2). Comparing these EOF patterns with the four SVD patterns of soil moisture, it seems that the 2nd EOF and the 1st SVD pattern are similar

Table 2. Statistics of EOF Analysis[a]

Modes, S	Modes, P	σ_S, %	σ_P, %	$r_{s,p}$, %
1	3	22.3	7.0	19.0
2	1	12.9	11.3	29.5
3	4	10.7	6.6	18.4
4	2	4.6	8.5	35.2

[a] S and P represent soil moisture and precipitation, respectively. σ is covariance, and $r_{S,P}$ is correlation coefficient of EOF expansion coefficient series between S and P.

to some extent. The 4th EOF and the 4th SVD pattern are similar to each other but their signs of anomalies are opposite (i.e., the 4th EOF has positive anomalies in a region where the 4th SVD has negative anomalies and vise verse).

[56] There are many similarities between the corresponding EOF patterns of precipitation (not shown) with those of soil moisture. The related statistics of precipitation EOF patterns is listed in Table 2. Note that, because the kth ($k = 1, 2, 3, 4$) EOF modes of soil moisture and precipitation do not necessarily correspond to each other, the order of the precipitation modes have been changed to $k = 3, 1, 4, 2$ to ensure that, in the new order, the kth mode of soil moisture has a relatively larger correlation with the jth mode of precipitation for $j = k$ than $j \neq k$.

[57] Figure 11 shows the time lag correlation coefficients between soil moisture and precipitation of the EOF expansion series. No correlation coefficient reaches the critical correlation (30%) at the 99.9% confidence level except for one case of precipitation leading soil moisture by one month. In addition, the simultaneous correlation coefficients of the EOF time series are 19–35%, only about 1/3 to 1/2 of those for SVD. These results clearly indicate the advantage of SVD over EOF patterns in connecting soil moisture to subsequent precipitation variability.

6. Concluding Remarks

[58] Singular value decomposition analysis has been conducted to identify the soil moisture spatial patterns closely related to monthly-seasonal precipitation variability in east Asia. The two hydrological fields were obtained from a simulation of a decade with the NCAR regional climate model. The results provide some insights into the importance of spatial patterns of soil moisture to prediction of monthly-seasonal variability of precipitation in the monsoon region.

[59] The results suggest that the predictability of monthly-seasonal precipitation variability could be improved by using soil moisture as a predictor in the form of its coupled SVD patterns with precipitation instead of the original data at individual locations. The SVD spatial patterns of soil moisture show much closer relationships with subsequent monthly-seasonal precipitation variability than the original data do. The relations in the form of SVD patterns are also more significant than those in the form of EOF patterns.

[60] The leading SVD modes of soil moisture in east Asia are categorized into two types according to their relationships with the atmospheric anomalies. Only those SVD patterns corresponding to the atmospheric anomalous patterns with opposite signs between the middle and low troposphere and with comparable magnitude in the anomalies over both middle latitudes and south-central China are found to have close relations to subsequent monthly-seasonal precipitation variability. The roles of this type of soil moisture SVD patterns are more significant in spring and summer seasons. To better understand physical significance of these types of SVD patterns, numerical experiments with a regional/global climate model are needed to investigate the responses of precipitation to initial soil moisture anomalies, with their spatial distribution specified based on the SVD patterns.

[61] A reliable simulation of the land-atmospheric hydrological processes is essential to understanding the importance of spatial patterns of soil moisture. As in other climate models, precipitation simulation is one of the processes with great uncertainties in RegCM. This certainly would further affect the simulation of soil moisture and the land-atmospheric interactions. Another uncertainty is from the snow simulation with RegCM. The version of the model used in this study [*Giorgi et al.*, 1993a, 1993b] was not coupled with an explicit snow scheme [e.g., *Yang et al.*, 1997]. The continuous efforts in developing parameterizations of precipitation and snow should be critical to improving simulation of atmospheric and soil hydrological processes.

[62] No observational validations are available for the simulated SVD spatial patterns of soil moisture in east Asia, basically due to the lack of soil moisture measurements for the simulation period (1988–1997). There are several soil moisture data sets for China. The one used in the work of *Entin et al.* [2000] and *Liu et al.* [2001] contains complete time series over a period of 11 years, but it covers a different period (1981–1991) from the simulation period. Another data set [*Liu et al.*, 1994] contains measurements at

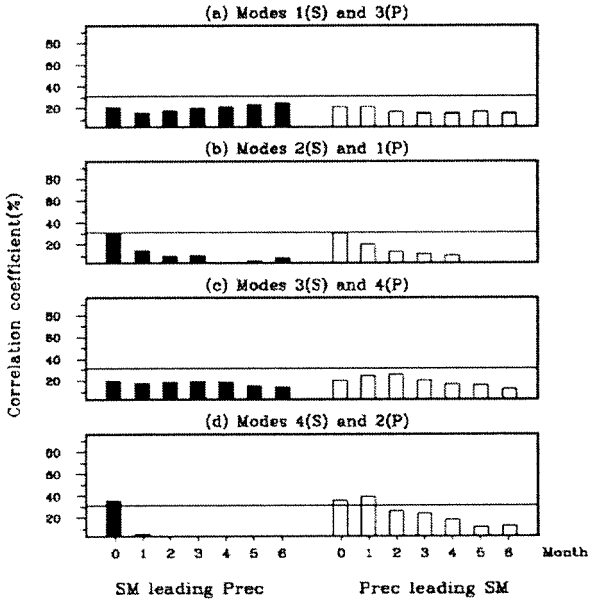

Figure 11. Time lag correlation coefficients between EOF expansion series for (left) soil moisture leading precipitation and (right) precipitation leading soil moisture. (a–d) The four EOF leading modes. The light line in each panel indicates the 99.9% confidence level.

hundreds of stations over a decade-long period. However, the data are discontinuous for northern China during cool seasons due to frozen soil. An alternate data set available in near future is the global soil moisture series calculated by land-surface hydrological models with observed precipitation from, e.g., the GEWEX/Global Land-Atmosphere System Study(GLASS) [*Dirmeyer*, 2002]. The application of measured precipitation is expected to produce more reliable soil moisture, though it is still a model product.

[63] SVD, similar to other principal component analysis (CPA) techniques like CCA and combined CPA (CCPA), identifies linear connections between two fields [*Bretherton et al.*, 1992]. The processes of soil moisture and precipitation variability and their interactions, however, are basically nonlinear, even at long-tem scales.

[64] **Acknowledgments.** The author would like to thank Roni Avissar and Hui Wang for valuable discussions. Hui Wang provided the SVD analysis computer code. The author also wish to thank three anonymous reviewers whose comments significantly improved the manuscript, and Gary Achtemeier whose editing improved writing of the manuscript. This research was supported by the National Aeronautics and Space Administration under grant NAG8-1513.

References

Anthes, R. A., A cumulus parameterization scheme utilizing a one-dimensional cloud model, *Mon. Weather Rev.*, *105*, 270–286, 1977.

Anthes, R. A., E.-Y. Hsie, and Y.-H. Kuo, Description of the Penn State/NCAR Mesoscale Model Version 4(MM4), *Tech. Note NCAR/TN-282+STR*, 66 pp., Natl. Cent. for Atmos. Res., Boulder, Colo., 1987.

Avissar, R., Recent advances in the representation of land-atmosphere interactions in global climate models, *Rev. Geophys.*, *33*, 1005–1010, 1995.

Avissar, R., and Y. Q. Liu, A three-dimensional numerical study of shallow convective clouds and precipitation induced by land-surface forcings, *J. Geophys. Res.*, *101*, 7499–7518, 1996.

Avissar, R., and M. M. Verstraete, The representation of continental surface processes in atmospheric models, *Rev. Geophys.*, *28*, 35–52, 1990.

Barnett, T. P., and R. Preisendorfer, Origins and levels of monthly and seasonal forest skill for United States surface air temperatures determined by conanical correlation analysis, *Mon. Weather Rev.*, *115*, 1825–1850, 1987.

Barnston, A. G., Linear statistical short-term climate predictive skill in the Northern Hemisphere, *J. Clim.*, *7*, 1513–1564, 1994.

Betts, A. K., J. H. Ball, A. C. M. Beljaars, M. J. Miller, and P. A. Viterbo, The land-surface-atmosphere interaction: A review based on observational and global modeling perspectives, *J. Geophys. Res.*, *101*, 7209–7226, 1996.

Bosilovich, M. G., and W.-Y. Sun, Numerical simulation of the 1993 midwestern flood: Land-atmosphere interactions, *J. Clim.*, *12*, 1490–1505, 1999.

Bretherton, C. S., C. Smith, and J. M. Wallace, An intercomparison of methods for finding coupled patterns in climate data, *J. Clim.*, *5*, 541–560, 1992.

Brubaker, K. L., and D. Entekhabi, Analysis of feedback mechanisms in land-atmosphere interaction, *Water Resour. Res.*, *32*, 1343–1357, 1996.

Dai, Y., et al., The Common Land Model (CLM), *Bull. Am. Meteorol. Soc*, in press, 2003.

Delworth, T., and S. Manabe, The influence of potential evaporation on the variabilities of simulated soil wetness and climate, *J. Clim.*, *1*, 523–547, 1988.

Delworth, T., and S. Manabe, The influence of soil wetness on near-surface atmospheric variability, *J. Clim.*, *2*, 1447–1462, 1989.

Dickinson, R. E., and A. Henderson-Sellers, Modeling tropical deforestation: A study of GCM land-surface parameterizations, *Q. J. R. Meteorol. Soc.*, *114*, 439–462, 1988.

Dickinson, R. E., R. M. Errico, F. Giorgi, and G. T. Bates, A regional climate model for the western U.S., *Clim. Change*, *15*, 383–422, 1989.

Dickinson, R. E., A. Henderson-Sellers, and P. J. Kennedy, Biosphere-Atmosphere Transfer Scheme (BATS) version 1E as coupled to the NCAR Community Climate Model, *Tech. Note TN-387*, 72 pp., Natl. Cent. for Atmos. Res., Boulder, Colo., 1993.

Ding, Y. H., Summer monsoon rainfall in China, *J. Meteorol. Soc. Jpn.*, *70*, 243–266, 1991.

Dirmeyer, P. A., Second GEWEX/GLASS Global Soil Wetness Project (GSWP2), paper presented at Mississippi River Climate and Hydrology Conference, New Orleans, La., NOAA Off. of Global Programs, Dep. of Energy Atmos. Radiat. Program, NASA Terr. Hydrol. Program, Am. Meteorol. Soc., 13–17 May 2002.

Eltahir, A. B., A soil moisture-rainfall feedback mechanism: 1. Theory and observations, *Water Resour. Res.*, *34*, 765–785, 1998.

Entekhabi, D., D. Rodriguez-Iturbe, and R. I. Bras, Variability in large-scale water balance with land surface-atmosphere interaction, *J. Clim.*, *57*, 798–813, 1992.

Entin, J. K., A. Robock, K. Y. Vinnikov, S. E. Hollinger, S. Liu, and A. Namkhai, Temporal and spatial scales of observed soil moisture variations in the extratropics, *J. Geophys. Res.*, *105*, 11,865–11,877, 2000.

Findell, K. L., and A. B. Eltahir, An analysis of the soil moisture-rainfall feedback, based on direct observations from Illinois, *Water Resour. Res.*, *33*, 725–735, 1997.

Giorgi, F., and G. T. Bates, The climatological skill of a regional model over complex terrain, *Mon. Weather. Rev.*, *117*, 2325–2347, 1989.

Giorgi, F., and X. Bi, A study of internal variability of a regional climate model, *J. Geophys. Res.*, *105*, 29,503–29,521, 2000.

Giorgi, F., and L. O. Mearns, Introduction to special section: Regional climate modeling revisited, *J. Geophys. Res.*, *104*, 6335–6352, 1999.

Giorgi, F., and C. Shields, Tests of precipitation parameterizations available in latest version of NCAR regional climate model (RegCM) over continental United States, *J. Geophys. Res.*, *104*, 6353–6375, 1999.

Giorgi, F., M. R. Marinucci, G. De Canio, and G. T. Bates, Development of a second generation regional climate model (RegCM2), I, Boundary layer and radiative transfer processes, *Mon. Weather Rev.*, *121*, 2794–2813, 1993a.

Giorgi, F., M. R. Marinucci, G. De Canio, and G. T. Bates, Development of a second generation regional climate model (RegCM2), II, Convective processes and assimilation of lateral boundary conditions, *Mon. Weather Rev.*, *121*, 2814–2832, 1993b.

Giorgi, F., L. O. Mearns, C. Shields, and L. Mayer, A regional model study of the importance of local versus remote controls of the 1988 drought and the 1993 flood over the central United States, *J. Clim.*, *9*, 1150–1162, 1996.

Hong, S.-Y., and H.-L. Pan, Impact of soil moisture anomalies on seasonal summertime circulation over North America in a regional climate model, *J. Geophys. Res.*, *105*, 29,625–29,634, 2000.

Huang, J., H. M. van den Dool, and P. K. Georgakakos, Analysis of model calculated soil moisture over the United States (1931–1993) and applications to long-range temperature forecasts, *J. Clim.*, *9*, 1350–1362, 1996.

Karl, T. R., The relationship of soil moisture parameterizations to subsequent seasonal and monthly mean temperature in the United States, *Mon. Weather Rev.*, *114*, 675–686, 1986.

Kiehl, J. T., J. J. Hack, G. B. Bonan, B. A. Boville, B. P. Briegleb, D. L. Williamson, and P. J. Rash, Description of the NCAR Community Climate Model (CCM3), *Rep. NCAR/TN-420+STR*, Natl. Cent. for Atmos. Res., Boulder, Colo., 1996.

Koster, R. D., and M. J. Suarez, The relative contributions of land and ocean processes to precipitation variability, *J. Geophy. Res.*, *100*, 13,775–13,790, 1995.

Koster, R. D., M. J. Suarez, and M. Heiser, Variance and predictability of precipitation at seasonal-to-interannual timescales, on precipitation, *J. Hydrometeorol.*, *1*, 26–46, 2000.

Lee, D.-K., and M.-S. Suh, Ten-year east Asian summer monsoon simulation using a regional climate model (RegCM2), *J. Geophys. Res.*, *105*, 29,565–29,577, 2000.

Liu, S., X. Mo, H. Li, G. Peng, and A. Robock, Spatial variation of soil moisture in China: Geostatistical characterization, *J. Meteorol. Soc. Jpn.*, *79*, 555–574, 2001.

Liu, Y., Prediction of monthly-seasonal precipitation using coupled SVD patterns between soil moisture and subsequent precipitation, *Geophys. Res. Lett.*, *30*(15), 1827, doi:10.1029/2003GL017709, 2003.

Liu, Y., and R. Avissar, A study of persistence in the land-atmosphere system using a general circulation model and conservations, *J. Clim.*, *12*, 2139–2153, 1999a.

Liu, Y., and R. Avissar, A study of persistence in the land-atmosphere system with a fourth-order analytical model, *J. Clim.*, *12*, 2154–2168, 1999b.

Liu, Y., F. Giorgi, and W. M. Washington, Simulation of summer monsoon climate over east Asia with an NCAR regional climate model, *Mon. Weather Rev.*, *122*, 2331–2348, 1994.

Liu, Y., R. Avissar, and F. Giorgi, A simulation with the regional climate model (RegCM2) of extremely anomalous precipitation during the 1991 east Asia flood: An evaluation study, *J. Geophys. Res.*, *101*, 26,199–26,215, 1996.

Mintz, Y., The sensitivity of numerically simulated climate to land-surface boundary conditions, in *The Global Climate*, edited by J. T. Houghton, pp. 79–105, Cambridge Univ. Press, New York, 1984.

Mo, K. C., Ensemble canonical correlation prediction of summer season precipitation over the United States, paper presented at Mississippi River

Climate and Hydrology Conference, New Orleans, La., NOAA Off. of Global Programs, Dep. of Energy Atmos. Radiat. Program, NASA Terr. Hydrol. Program, Am. Meteorol. Soc., 13–17 May 2002.

Pal, J. S., and E. A. B. Eltahir, Pathway relating soil moisture conditions to future summer rainfall within a model of the land-atmosphere system, *J. Clim.*, *14*, 1227–1242, 2001.

Parnston, A. G., Linear statistical short-term climate predictive skill in the Northern Hemisphere, *J. Clim.*, *8*, 1513–1564, 1994.

Rodriguez-Iturbe, I., D. Entekhabi, and R. I. Bras, Nonlinear dynamics of soil moisture at climate scales: 1. Stochastic analysis, *Water Resour. Res.*, *27*, 1899–1906, 1991.

Schar, C., D. Luthi, U. Beyerle, and E. Heise, The soil-precipitation feedback: A process study with a regional climate model, *J. Clim.*, *12*, 722–741, 1999.

Seth, A., and F. Giorgi, The effects of domain choice on summer precipitation simulation and sensitivity in a regional climate model, *J. Clim.*, *11*, 2698–2712, 1998.

Shea, D. J., K. E. Trenberth, and R. W. Reynolds, A global monthly sea surface temperature climatology, *J. Clim.*, *5*, 987–1001, 1992.

Ting, M. F., and H. Wang, Summertime United States precipitation variability and its relation to Pacific sea surface temperature, *J. Clim.*, *10*, 1853–1873, 1997.

Trenberth, K. E., D. P. Stepaniak, and J. M. Caron, Interannual variations in the atmospheric heat budget, *J. Geophys. Res.*, *107*(D8), 4066, doi:10.1029/2000JD000297, 2002.

Vinnikov, K., A. Robock, N. A. Speranskaya, and C. A. Schlosser, Scales of temporal and spatial variability of midlatitude soil moisture, *J. Geophys. Res.*, *101*, 7163–7174, 1996.

Wallace, J. M., C. Smith, and C. S. Bretherton, Singular value decomposition of wintertime sea surface temperature and 500-mp height anomalies, *J. Clim.*, *5*, 561–576, 1992.

Wang, H., and M. F. Ting, Covariability of winter U.S. precipitation and Pacific sea surface temperatures, *J. Clim.*, *15*, 3711–3719, 2000.

Wang, W. Q., and A. Kumar, A GCM assessment of atmospheric seasonal predictability associated with soil moisture anomalies over North America, *J. Geophys. Res.*, *103*, 28,637–28,646, 1998.

Yang, Z.-L., R. E. Dickinson, A. Robock, and K. Y. Vinnikov, On validation of the snow submodel of the biosphere-atmosphere transfer scheme with Russian snow cover and meteorological observational data, *J. Clim.*, *10*, 353–373, 1997.

Zeng, X., R. E. Dickinson, A. Walker, M. Shaikh, R. S. DeFries, and J. Qi, Derivation and evaluation of global 1-km fractional vegetation cover data for land modeling, *J. Appl. Meteorol.*, *39*, 826–839, 2000.

Y. Liu, Forestry Sciences Laboratory, USDA Forest Service, 320 Green St., Athens, GA 30602, USA. (yliu@fs.fed.us)